3D direct laser writing using a 405 nm diode laser

Patrick Mueller,[1,2,3,*] Michael Thiel,[2] and Martin Wegener[1,3]

[1]*Institute of Nanotechnology, Karlsruhe Institute of Technology (KIT), Karlsruhe 76128, Germany*

[2]*Nanoscribe GmbH, Eggenstein-Leopoldshafen 76344, Germany*

[3]*Institute of Applied Physics, Karlsruhe Institute of Technology (KIT), Karlsruhe 76128, Germany*

**Corresponding author: pat.mueller@kit.edu*

Received October 10, 2014; accepted October 29, 2014;
posted November 4, 2014 (Doc. ID 224514); published December 9, 2014

Three-dimensional (3D) direct laser writing commonly uses near-infrared femtosecond laser pulses. Here, we use a quasi-cw blue diode laser at a 405 nm wavelength. As prerequisite, we identify photoresist systems that unambiguously show nonlinear multiphoton polymerization at this excitation wavelength. Next, we obtain a diffraction-limited focus with a high-numerical-aperture objective lens (NA = 1.4), which is crucial to actually benefit from the wavelength advantage. To evaluate the anticipated reduced linewidths and improved resolution, we fabricate and characterize 2D and 3D benchmark structures. Finally, we also demonstrate dip-in direct laser writing with our setup.

OCIS codes: (350.3390) Laser materials processing; (160.5298) Photonic crystals; (160.5293) Photonic bandgap materials; (050.6875) Three-dimensional fabrication; (110.6895) Three-dimensional lithography; (330.6130) Spatial resolution.

http://dx.doi.org/10.1364/OL.39.006847

Progress in optical lithography has often been connected with a reduction of exposure wavelength. For example, the semiconductor industry has enabled the manufacturing of increasingly advanced and miniaturized microelectronic devices along these lines. After a period of improvements of process technologies for 193 nm, the next wavelength step will be taken within the next years with the advent of the extreme UV technology working at a wavelength of 13.5 nm [1].

Another relevant optical lithography technique is direct laser writing (DLW) based on multiphoton polymerization. DLW has become a versatile and established fabrication technology for three-dimensional (3D) micro- and nanostructures [2] (also see the reviews [3–5]). Due to a wide range of applications in different disciplines, the number of users is rapidly increasing. In a DLW instrument, a laser beam with wavelength λ is tightly focused into the volume of a transparent photosensitive material (i.e., the linear absorption at λ is negligibly small). The material, typically a monomer-based negative-tone photoresist, changes its solubility upon exposure by multiphoton excitation (see below). Unexposed material is selectively washed out in a subsequent development step.

Just like for optical lithography in the semiconductor industry, the resolution of DLW depends on the excitation wavelength λ. The vast majority of authors have used femtosecond lasers around 800 nm for excitation. However, there are several reports on DLW setups using smaller wavelengths (e.g., $\lambda = 600$ nm [6,7] or $\lambda =$ 513–540 nm [5,8–14], or $\lambda = 442$ nm [15]). However, the achievable resolution and feature sizes have often not been investigated thoroughly or directly compared with the diffraction limit. More recently, stimulated-emission-depletion (STED)-inspired 3D DLW schemes have been reported (see, e.g., the extensive review [16]), conceptually and practically allowing for 3D optical lithography with performance beyond ordinary DLW, at the price of a significantly increased system complexity.

Here, we demonstrate 3D DLW at the short-wavelength end of the visible spectrum at a 405 nm wavelength. We fabricate and characterize 2D and 3D benchmark structures with periods at the diffraction limit corresponding to this wavelength.

Before we start discussing our experiments, we briefly revisit nonlinear photopolymerization: Typically, a photoresist is assumed to behave according to the threshold model, stating that the resist (i) locally accumulates consecutive exposure doses and (ii) can be solved during the development process unless the accumulated dose exceeds a certain threshold value [15]. In the case of a strictly linear process, it can easily be shown that it is fundamentally impossible to create arbitrary 3D structures as the volume in front of and behind the focal spot collects the same dose as the focal volume. In contrast, in the case of a nonlinear process of order $N > 1$ (e.g., two-photon absorption ($N = 2$)) the exposure dose is proportional to I^N, with I being the laser intensity. The nonlinearity suppresses off-focal components so that only the focal volume accumulates a considerable nonzero exposure dose, leading to a spatially confined writing volume called a voxel. Note, however, that the source of the nonlinearity does not necessarily have to lie in the optical absorption process but can also be due to other effects (e.g., oxygen-scavenging free radicals [15,17]). Accordingly, as a prerequisite, we need to find a photoresist system that shows an effectively nonlinear behavior at a 405 nm wavelength.

For our experiments, we use a commercial DLW instrument (Nanoscribe Photonic Professional) and a quasi-continuous wave (cw) diode laser (Toptica iBeam smart 405S, 300 mW), which is fiber-coupled into the eyepiece port of the microscope (similar to [18]). For focusing, we use a Zeiss objective lens with a numerical aperture of 1.4 and 100× magnification. To determine the effective nonlinearity of different photoresist compositions, we vary the repetition rate, R, of the electronically pulsed laser diode and follow a scheme similar to [19] (also see the discussion of other approaches to determine N in Section 4 of [19]). We recall that the exposure dose follows $D \propto R \cdot \Delta t \cdot I_p^N$, where Δt is the pulse length and I_p is the peak intensity of the pulses.

The threshold peak power, which is proportional to the threshold pulse peak intensity, becomes $P_{\mathrm{th}} \propto (R\Delta t)^{-1/N}$. Thus, the nonlinearity can be measured directly by varying R or Δt and determining the respective threshold laser power. The latter is varied in discrete equidistant steps. R and Δt effectively change the dimensionless duty cycle $q = R\Delta t$ of the pulse scheme. Specifically, we write lines 10 μm in length with a writing speed of 100 μm/s and develop them by mr-dev 600 (microresist technology) followed by rinsing with isopropanol and blowing with nitrogen. The corresponding polymerization threshold powers are determined by inspection via a dark-field light microscope. Figure 1(a) shows the results for three different resist systems that we have studied. All three are used as received (i.e., no further modification or purification is performed). First, we examine pentaerythritol triacrylate (PETA), a monomer commonly used for DLW [16,17], mixed with 1 wt. % of the photoinitiator Irgacure 500 (BASF AG), which shows negligible absorption at 405 nm according to its data sheet. However, the linear fit results in a value of $N = 1.12 \pm 0.05$ (i.e., close to linear behavior), which we attribute to a dominant one-photon absorption by the photoinitiator. All efforts to fabricate general 3D structures with this mixture failed (not depicted). Second, the pure monomer without any photoinitiator is investigated. To our surprise, it can be polymerized efficiently anyway. While the threshold powers are considerably higher than with the initiator, a value of $N = 1.61 \pm 0.09$ can be found, suitable for 3D structuring. Third, IP-Dip without photoinitiator is examined (commercially available, Nanoscribe). Compared to pure PETA, it shows an even larger nonlinearity of $N = 1.84 \pm 0.04$ as well as lower threshold powers. As a measure for the processing window, Fig. 1(b) shows the dynamic range for both useful nonlinear resists. The dynamic range r is defined as $r = P_{\mathrm{dam}}/P_{\mathrm{th}} - 1$, with P_{dam} being the laser peak power at which microexplosions occur due to heat accumulation [19]. IP-Dip shows significantly higher values for r (i.e., it is less prone to erratic microexplosions), enabling robust DLW operation. We thus consider this resist as the most useful one found so far. It is beyond the scope of this Letter to understand the underlying chemical or physical processes, but we speculate that the effective nonlinearity of this resist stems from the photolysis of organic bonds [20].

In order to benefit from the anticipated resolution advantage due to the shorter exposure wavelength, it is crucial to achieve a diffraction-limited laser focus. At wavelengths as low as 405 nm, this is not simple for standard microscope objective lenses. We compare with a simulation following [21] that shows the expected diffraction-limited beam taking into account the properties of the objective lens, the beam polarization, and the beam diameter. We measure the point-spread function by scanning 100 nm diameter gold beads through the focus. The results of the calculation and experiment are depicted in Fig. 2(a). From the good agreement we conclude that a close to diffraction-limited laser focus is achieved. Fitting with a Gaussian, the full width at half-maximum values are 200, 175, and 450 nm in the x, y, and z direction. By employing Sparrow's criterion [16] and taking the intensity distribution to the power of $N = 1.84$ for IP-Dip, these values correspond to the smallest lithographically resolvable distances of $a_x = 128$ nm, $a_y = 112$ nm, and $a_z = 287$ nm.

The lateral resolution is examined experimentally by writing 2D structures onto the glass substrate surface. We choose a repetition rate of $R = 1$ MHz and duty cycles of $q = 5$–10%. We write line gratings with a writing speed of 100 m/s. The grating period is varied in steps of 10 nm. To rule out dynamic effects of the piezo stage, we also write point arrays, where each point is exposed for a total time of 4 ms while the stage is at rest. To compensate for variations in interface detection and possible drifts of the substrate, we write the structures at different z positions. The development is as described above. Figure 2(b) shows scanning electron microscope (SEM) images of typical writing results. For both line gratings and point arrays, well-separated features are found for periods as small as $a = 120$ nm. Structures with $a = 110$ nm can only be completely resolved when writing

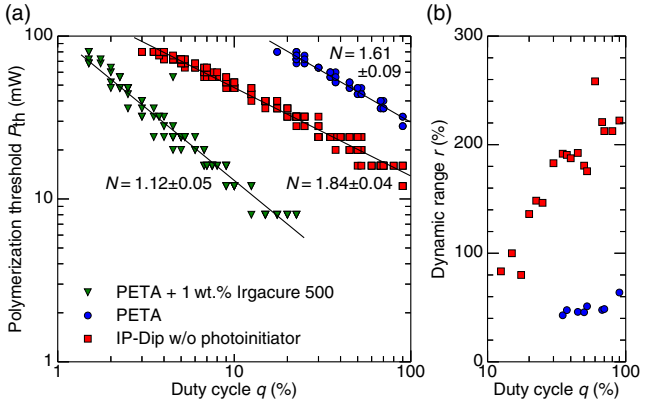

Fig. 1. (a) Polymerization threshold powers versus duty cycle for three different photoresists. In this double-logarithmic plot, the slopes of the fitted straight lines yield the effective nonlinearity N. (b) The dynamic range (as defined in the text) versus duty cycle for the two useful photoresists exhibiting nonlinear behavior.

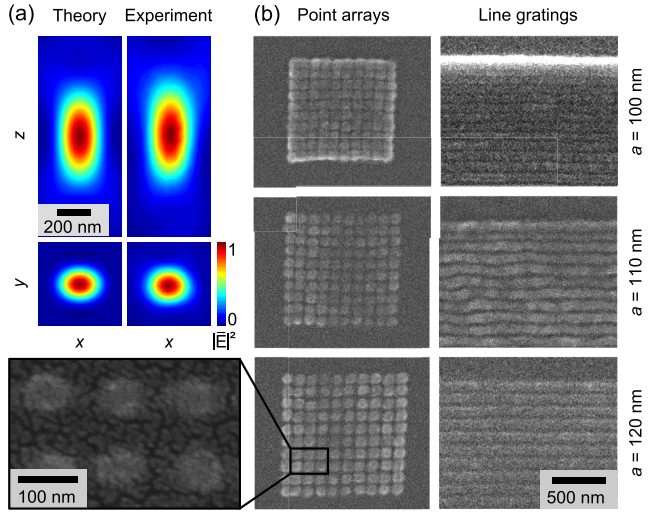

Fig. 2. (a) Calculated and measured laser focus at a 405 nm wavelength. (b) Electron micrographs of fabricated 2D test structures for different periods close to the resolution limit. Photoresist is IP-Dip without photoinitiator.

very close to the polymerization threshold, leading to low yield and deteriorations of the structure shapes, especially for line gratings. At $a = 100$ nm it turns out to be impossible to fabricate clearly separated structures. Thus, we conclude that the experimentally achieved minimum laterally resolvable distance is 110 nm, which fits nicely to our predicted values above. These results show the best lateral resolution reported for diffraction-limited DLW (without "taking advantange" of shrinkage effects) and also outperform recent results by 3D STED DLW [16,22]. Concerning minimum feature sizes we find line widths as low as 78 nm as well as point diameters of 50 to 70 nm.

The experimental determination of the axial resolution limit is more involved. Often in the literature individual lines or voxels are studied, but it is our experience that polymeric structures not attached to the substrate show considerable shrinkage during electron microscopy that may lead to the wrong results. Instead, we fabricate woodpile photonic crystals [23], which are true 3D structures and have become a standard benchmark structure in the field [8,6,10,16]. These structures consist of layers of parallel rods separated by a lateral period or lattice constant a where each layer is rotated by 90° and shifted by $a/2$ with respect to the one below. This leads to an axial period consisting of four layers with an axial lattice constant of $c = \sqrt{2} \cdot a$. If the critical distance of $3/4 \cdot c$ is resolved by the DLW process, the structures show a photonic stopband with a spectral position depending on their dimensions. Our woodpile structures contain 20 layers and have a footprint of 40 μm × 40 μm. The rod spacing a is varied in steps of 25 nm. To precompensate for shrinkage, the structures are axially stretched by 30% [16] (i.e., we increase the critical distance to $a_{\text{crit}} = 3/4 \cdot 1.3 \cdot c$).

Figure 3(a) shows an SEM image of a woodpile structure with $a = 250$ nm. The rods are nicely aligned, have constant width, and show only neglible distortions. The smallest line width is 68 nm. The inset shows a focused-ion-beam (FIB) cut through the same structure. Apart from the rod tips being deformed and shrunk by the cutting process, it is evident that the layers are well separated in the axial direction and that the structure also shows good quality in its center. In Fig. 3(b) the corresponding transmittance and reflectance spectra are depicted, which are taken prior to SEM imaging using a commercial Fourier-transform infrared (FTIR) spectrometer (Bruker Equinox 55). The transmittance decreases to 60% for wavelengths around 425 nm, while the reflectance spectrum shows a peak reflectance of about 50%. As shown in the inset, the structure appears blue in the microscope under reflection-mode imaging. These effects evidence a photonic stopband around 425 nm wavelength that prevents the respective waves from propagating through the crystal. In our experiments the woodpile structures showing a photonic stopband can be fabricated in good quality with lattice constants as low as $a = 250$ nm. Taking into account the shrinkage compensation mentioned above, we thus find the axial resolution limit to be 345 nm, which is 20% higher than expected from the measured focus. We attribute this deviation to more complex shrinkage effects that have not been corrected by our rather simple compensation approach. Nevertheless, to the best of our knowledge, this is the highest axial resolution demonstrated for woodpiles made by 3D DLW. Our results even outperform our previous best values obtained by 3D STED DLW [16].

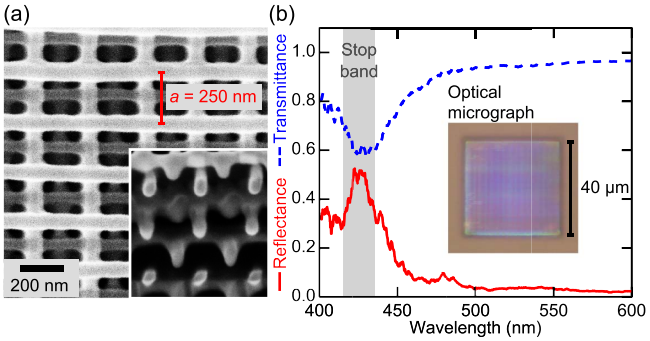

Fig. 3. (a) Top view electron micrograph of a woodpile photonic crystal with a rod spacing of $a = 250$ nm. The inset shows an oblique view of a focused-ion-beam cut through the structure. (b) Reflectance and transmittance spectra of the same structure obtained by FTIR measurements indicating a photonic stopband. The inset is a reflection-mode optical micrograph of the structure, exhibiting the corresponding blue appearance. Photoresist is IP-Dip without photoinitiator.

Finally, we test our setup by making larger overall structures. For fabricating heights in the range of a few to hundreds of micrometers, writing in an oil-immersion microscopy setup is not suitable anymore because (i) the maximum height of structures is limited by the working distance of the objective lens and (ii) writing through already polymerized regions leads to focus deviations and stimulation of microexplosions. Dip-in DLW [24] circumvents these restrictions by using the photoresist itself as immersion medium. We can adapt this writing scheme in our setup with minimal changes. We again use IP-Dip photoresist and the same writing conditions as above for the woodpile structures. The writing results of the different test structures are depicted in Fig. 4 and show that the dip-in scheme also works very well at 405 nm. This altogether enables the fabrication of structures spanning several orders of magnitude in size.

In conclusion, we have investigated a 3D DLW scheme based on a quasi-cw 405 nm wavelength diode laser. Compared to femtosecond lasers, diode lasers are less expensive, even more reliable, and allow for direct power modulation (i.e., an acousto-optic modulator is not

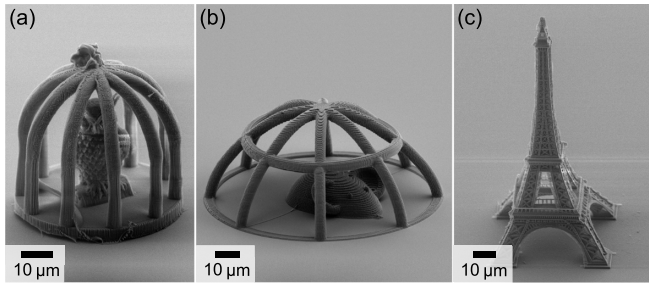

Fig. 4. Electron micrographs of different 3D structures fabricated by dip-in direct laser writing with 405 nm excitation wavelength. Photoresist is IP-Dip without photoinitiator.

necessary). We have achieved a close to diffraction-limited laser focus and have identified a suitable photoresist by nonlinearity measurements. We have achieved point diameters as small as 50 nm, 2D line gratings with 110 nm lateral period, and 3D woodpile photonic crystals with 250 nm rod spacing, equivalent to 345 nm axial resolution. These values compare favorably with previous DLW work, even including 3D STED-inspired DLW approaches. Besides benchmarking our system, we have also employed a dip-in writing scheme and have fabricated a variety of microstructures to illustrate the versatility. Further reduction of the exposure wavelength to below 400 nm might lead to further resolution improvements, but this would require dedicated focusing optics and new photoresists that are still transparent in the UV.

We acknowledge support from the Nanoscribe R&D team and many fruitful discussions with fellow group members. We thank the Karlsruhe School of Optics & Photonics (KSOP) and the Helmholtz International Research School (HIRST) for support.

References

1. C. Wagner and N. Harned, Nat. Photon. **4**, 24 (2010).
2. S. Kawata, H.-B. Sun, T. Tanaka, and K. Takada, Nature **412**, 697 (2001).
3. S. Maruo and J. Fourkas, Laser Photon. Rev. **2**, 100 (2008).
4. G. von Freymann, A. Ledermann, M. Thiel, I. Staude, S. Essig, K. Busch, and M. Wegener, Adv. Funct. Mater. **20**, 1038 (2010).
5. M. Malinauskas, M. Farsari, A. Piskarskas, and S. Juodkazis, Phys. Rep. **533**, 1 (2013).
6. L. Nguyen, M. Straub, and M. Gu, Adv. Funct. Mater. **15**, 209 (2005).
7. N. Pucher, A. Rosspeintner, V. Satzinger, V. Schmidt, G. Gescheidt, J. Stampfl, and R. Liska, Macromolecules **42**, 6519 (2009).
8. M. Straub and M. Gu, Opt. Lett. **27**, 1824 (2002).
9. I. Wang, M. Bouriau, P. L. Baldeck, C. Martineau, and C. Andraud, Opt. Lett. **27**, 1348 (2002).
10. W. Haske, V. W. Chen, J. M. Hales, W. Dong, S. Barlow, S. R. Marder, and J. W. Perry, Opt. Express **15**, 3426 (2007).
11. M. Thiel, J. Fischer, G. Von Freymann, and M. Wegener, Appl. Phys. Lett. **97**, 221102 (2010).
12. E. T. Ritschdorff and J. B. Shear, Anal. Chem. **82**, 8733 (2010).
13. A. Ovsianikov, A. Deiwick, S. Van Vlierberghe, M. Pflaum, M. Wilhelmi, P. Dubruel, and B. Chichkov, Materials **4**, 288 (2011).
14. C. De Marco, A. Gaidukeviciute, R. Kiyan, S. M. Eaton, M. Levi, R. Osellame, B. N. Chichkov, and S. Turri, Langmuir **29**, 426 (2013).
15. S. Maruo and K. Ikuta, Appl. Phys. Lett. **76**, 2656 (2000).
16. J. Fischer and M. Wegener, Laser Photon. Rev. **7**, 22 (2013).
17. J. B. Mueller, J. Fischer, F. Mayer, M. Kadic, and M. Wegener, Adv. Mat. **26**, 6566 (2014).
18. M. Thiel, J. Ott, A. Radke, J. Kaschke, and M. Wegener, Opt. Lett. **38**, 4252 (2013).
19. J. Fischer, J. B. Mueller, J. Kaschke, T. J. Wolf, A.-N. Unterreiner, and M. Wegener, Opt. Express **21**, 26244 (2013).
20. W. Knolle, T. Scherzer, S. Naumov, and R. Mehnert, Radiat. Phys. Chem. **67**, 341 (2003).
21. A. Van de Nes, L. Billy, S. Pereira, and J. Braat, Opt. Express **12**, 1281 (2004).
22. R. Wollhofen, J. Katzmann, C. Hrelescu, J. Jacak, and T. A. Klar, Opt. Express **21**, 10831 (2013).
23. K. Ho, C. Chan, C. Soukoulis, R. Biswas, and M. Sigalas, Solid State Commun. **89**, 413 (1994).
24. T. Bückmann, N. Stenger, M. Kadic, J. Kaschke, A. Frölich, T. Kennerknecht, C. Eberl, M. Thiel, and M. Wegener, Adv. Mat. **24**, 2710 (2012).